Localization of PLEKHO2 During Phagocytosis: Investigating potential relationships with CAPZA and PIP2

Mingzhu Zhao

MBT Biotechnology

Supervisors:

Daan Vorselen

Youri Peeters

Cell Biology and Immunology (CBI)

Wageningen university & Research

March 2025

Abstract

Phagocytosis, a vital cellular process executed primarily by professional phagocytes (monocytes, macrophages, neutrophils, and dendritic cells), is essential for eliminating microorganisms and apoptotic cells, thus maintaining tissue homeostasis. Impaired phagocytosis can lead to recurrent infections and severe diseases. During phagocytosis, the phagocytic cup membrane recruits various mediators, including PLEKHO2 (pleckstrin homology domain-containing family O member 2), a protein of unknown function. We hypothesized that PLEKHO2 functions by directing effector proteins to the cell membrane, such as capping protein (CapZ, regulates actin filament assembly and organization), via its binding affinity to cell membrane phosphatidylinositol phosphates (PIPs). Through electroporation of eGFP-tagged protein reporters into RAW264.7 macrophages, followed by phagocytosis assays, we were able to visualize the subcellular localization of the proteins of interest during the process of phagocytosis, and the association with F-actin was quantified using Pearson correlation coefficient. Here we identified localization of PLEKHO2 in phagocytic cups at various stages of phagocytosis, where it colocalized with F-actin and had a potential close relationship with CapZ, indicating a likely functional role of PLEKHO2 in phagocytosis. PIP2 exhibited increased distribution and colocalization with F-actin in early-stage phagocytic cups but dissociated from F-actin in late-stage cups, highlighting the need for a more dynamic method to investigate the relationship with PLEKHO2. In general, this research laid a foundation for further studies into PLEKHO2 as its role in phagocytosis was identified. Elucidating PLEKHO2's mechanisms in phagocytosis could enhance our understanding of immune cell function and potentially reveal new therapeutic targets for conditions involving defective phagocytosis, such as sepsis and neurodegeneration.

Introduction

Phagocytosis is an important cellular process for eliminating micro-organisms and apoptotic cells and is essential in maintaining tissue homeostasis (Hirayama et al., 2017). Professional phagocytes, namely monocytes, macrophages, neutrophils and dendritic cells, are the main executors of phagocytosis. Defective phagocytes can cause recurrent infections and tissue malfunctioning leading to further severe diseases (Boada-Romero et al., 2020). Hence, unravelling the molecular mechanisms involved in phagocytosis is crucial to understand the underlying malfunctioning and to treat and cure phagocytic related diseases.

Phagocytosis is composed of three sequential steps: recognition, engulfment and degradation (Uribe-Querol & Rosales, 2024). First, targets of various origins are recognized either by nonopsonic or opsonic receptors (Galloway et al., 2019). Activation of these receptors leads to F-actin polymerization and cytoskeleton rearrangement to start engulfment of targets by forming phagocytic cups (Aderem & Underhill, 1999), which is regulated by multiple proteins. When the target is fully engulfed, the phagosome matures and ultimately fuses with lysosomes to degrade the target (Donnelly & Barnes, 2012). One important group of cell membrane compounds, phosphoinositides (PIPs), was reported to play a crucial role throughout phagocytosis. Phosphatidylinositol 4,5-bisphosphate (PIP2) accumulates in the phagocytic cup, initiating phagocytosis, while its levels decrease as phagosomes form, converting to phosphatidylinositol 3,4,5-trisphosphate (PIP3) and other metabolites (Gillooly et al., 2001). PIP3 then appears on early phagosomes, crucial for maturation, and is later replaced by phosphatidylinositol 4-phosphate (PI4P) during the transition to late phagosomes. These dynamic PIP transitions regulate key events in phagocytosis by recruiting specific effector proteins and modulating F-actin dynamics (Levin et al., 2015; Vieira et al., 2001). Especially, PIP2 serves as a key signaling molecule during phagocytosis, recruiting diverse proteins to the cell membrane, including many that contain Pleckstrin homology (PH) domains (Lemmon et al., 1996). PH domain is the 11th most common domain in the human proteome, with its presence found in more than 11% of the proteins (Powis et al., 2023). One of the most important features of the PH domain is to bind PIPs, and thereby to guide proteins to the cellular membrane, despite the underlying mechanisms of specific interaction and regulation remain elusive (Powis et al., 2023).Recently, numerous genes involved in phagocytosis were identified by genome-wide CRISPR-screens (Vorselen et al., 2022). Among many known and new regulators of phagocytosis, a strong hit was the single PH domain containing protein, PLEKHO2 (pleckstrin homology domain-containing family O member 2). While PLEKHO2 remains largely unknown, recent studies have revealed its multifaceted roles in cellular processes and disease. Genetic variations in PLEKHO2 have been strongly associated with the development of type 2 diabetic retinopathy in a Taiwanese population (C. Han et al., 2012). Additionally, PLEKHO2 has been identified as a crucial factor in cell survival mechanisms. It inhibits TNFα-induced cell death by suppressing RIPK1 activation (Zhou et al., 2021) and promotes the survival of bone marrow-derived macrophages (Zhang et al., 2017).

Based on the identified characteristic PIP-binding ability of PH domains, we proposed that PLEKHO2, with its single PH domain, interacts with PIPs during phagocytosis, potentially guiding the localization of effector proteins. Additionally, with the aid of affinity chromatography – mass spectrometry, a potential interaction between PLEKHO2 and capping protein (CapZ) was identified (Cho et al., 2022). CapZ, a heterodimeric protein composed of α and β subunits, caps the barbed ends of F-actin filaments, preventing further polymerization or depolymerization, which is critical for regulating the actin cytoskeleton (Edwards, 2014). CapZA1 and CapZB are more noteworthy due to their strong hits in the genome-wide CRISPR-screens experiment that also identified a role of PLEKHO2 (Vorselen et al., 2022). Since determining a protein's subcellular localization is a crucial first step in inferring its function and identifying its interaction partners, further elucidating its role in cellular processes, our main goal in this study was to localize PLEKHO2 and investigate its colocalization with CAPZA and PIP2 during phagocytosis. Here, we first established a methodology to investigate the localization of a protein during phagocytosis by electroporating RAW 264.7 cells with one type of plasmid to express this protein tagged by fluorescent protein, followed by confocal microscopy to visualize spatial association with stained F-actin. To quantify the results, Pearson correlation coefficients of the protein of interest with F-actin in phagocytic cups at various stages were determined. This study established a foundation for elucidating PLEKHO2's role in phagocytosis by characterizing its localization and identifying potential interaction partners.

Material and methods

Plasmid extraction

Luria Bertani (LB) medium was prepared with 1% tryptone (Gibco, Cat. No. 211705), 0.5% yeast extract (Gibco, Cat. No.212750), 5 g NaCl (Merck, S9888-25G), 1 mole/liter NaOH (Merck, 1064980500) in MiliQ water before autoclaving. Antibiotic ampicillin (Thermofisher, Cat. No. J60977.14)/kanamycin (Thermofisher, Cat. No. 11815024) were added after LB medium autoclavation according to selective resistance marker inserted in each plasmid. Bacterial glycerol stocks for all the types of plasmids used (plasmid #13031, # 21179, #89245, Figure A1) were all available at the Cell Biology and Immunology department (Wageningen University and Research). A small amount of the stocks was taken using a sterile inoculation loop and added to the LB broth supplemented with the appropriate antibiotic and incubated overnight using shaking incubator (IKA Shakers KS 4000 i control) at spinning speed 220rpm. The next day, bacterial cells were pelleted by centrifugation before plasmid extraction using QIAGEN Plasmid Mini Kit (12123). Plasmid concentration and purity were assessed using Implen NanoPhotometer (N50/N60).

Electroporation optimization

Mock electroporation was performed using the Bio-Rad Gene Pulser (linear electroporation, 950 µF capacitance) without plasmid, applying electroporation voltages ranging from 175 V to 275 V in 25 V

increments on RAW 264.7 cells suspended in Opti-mem (Thermofisher, Cat No. 31985070) at a concentration of 10,000,000 cells/ml (or as specified) in a 0.4 mm cuvette. After incubating for 48 h, the RAW 264.7 cells were scraped off and transferred through a FACS tube with cell-strainer cap (Falcon CAT No. 352235) to ice-cold PBS prior to cell viability analysis using Cytoflex flow cytometer (Beckman Coulter) for their forward scatter (FSC), side scatter (SSC), and DRAQ7 intensity (wavelength: 678 nm). The data was processed via FlowJo (v.10.9.0) and cell viability was assessed as the ratio of living cells to the total number of detected cells, as determined by flow cytometry. The results were compared to a control group that was not subjected to electroporation. Next, varying plasmid quantities (3 µg, 10 µg, 20 µg per cuvette) of eGFP plasmid were incubated with the RAW cells for 10 min at room temperature followed by exposure to either 200 V or 275 V. Cell viability and eGFP-expressing cell percentage (488 nm excitation) were normalized to living cells in the 200 V control group (no plasmid). Afterward, we selected 250 V and 275 V (with 10 µg plasmid) for the next experiment. The optimized parameters were utilized for the subsequent electroporation of all the eGFP-tagged proteins of interest.

Cell cultivation

RAW 264.7 cell line was available at the Cell Biology and Immunology department (Wageningen University and Research). The cells were cultured and maintained at 37 °C incubator with 5% CO2 in RPMI-1640 medium (Thermofisher, Cat. No. 11875093) containing 10% Fetal Bovine Serum (Thermofisher, Cat. No. 10270106) and 100X antibiotic-antimycotics (Thermofisher, Cat No. 15240-062). Scraping was applied to detach cells for further purposes.

Functionalization of DAAM-particles

DAAM-particles were in stock ready to use for this study (synthesization process detailed in Vorselen et al. (2020). First, the DAAM-particle stock (6.5 kPa in stiffness, 8.6 mm in size) was diluted to 5% (v/v) and washed twice in activation buffer (100 mM MES, Acros organics, Cat. No. 397351000, 200 mM NaCl, pH 6.0, 10000g x 1min) and diluted in PBS (pH 7.4) Next, the DAAM-particles were incubated with 0.1% (v/v) tween, ethyl-3-(3-dimethylaminopropyl) carbodiimide (EDC (Sigma-Aldrich, Cat. No. E7750), 40 mg/ml), and N-hydroxysuccinimide (NHS, Thermo Scientific, Cat. No. A10312.22, 20 mg/ml) for 15 minutes at RT while mixing on an end-to-end rotator. After washing 3 times (0.1x PBS (pH 6) + 0.2% tween 20), DAAM-particles were resuspended in half of the original volume and the same volume of 2x PBS (pH 8.5) was added. After mixing, BSA (Roche, Cat. No. 10735086001, 200 mg/ml) was added prior to 1 h incubation on an end-to-end rotator. Then the entire DAAM-particles-BSA solution was transferred to a tube containing 5/6-TAMRA cadaverine ((Invitrogen, Cat. No. A1318)0.2 mM final concentration) followed by 30 minutes of incubation at RT using an end-to-end rotator. Finally, Tris buffer (Invitrogen, Cat. No. 15504020) with 300 mM ethanolamine (Sigma-Aldrich, Cat. No. E9508) was added in for blocking before another 30-min incubation section using an end-to-end rotator. The functionalized DAAM-particles were washed thrice

(pH 7.4, 0.1% tween 20) and further functionalized with anti-BSA antibody (IgG (MP Biomedicals, 0865111), 0.1 mg/ml final concentration) by 1 h incubation at RT using an end-to-end incubator. Lastly, the DAAM-particles were washed 3 times using PBS (pH 7.4) of the functionalized DAAM-particles before being stored at 4 °C.

Phagocytosis assay and F-actin staining

Cells were seeded in flat-bottom 96-well plates (cellvis, P96-1.5 H.N) at a density of 12,000, 15,000, 18,000 cells per well (3 wells per density) in cultivation buffer and incubated for 48 h at 37°C. The following day, medium in each well was replaced with 100 µl of cultivation buffer containing DAAM-particles at a concentration of 150,000 particles/ml, resulting in 15,000 particles per well. Plate was then centrifuged at 300 g for 1 min and incubated at 37°C for various time points (10, 20, and 30 minutes). At the last time point, fixed cells of entire plate by replacing cultivation buffers with fixative solution (4% paraformaldehyde (PFA, Thermo Scientific, Cat. No. 28908) in PBS, pH 7.4). And incubated for 10 min at room temperature followed by 3 washes with PBS to remove loose DAAM-particles. To permeabilize cells, replaced PBS with 0.2 % Triton X-100 (Merck, Cat. No. 108603, pH 7.4) and incubated for 10 min at room temperature followed by three PBS washes (pH 7.4). Lastly, replaced PBS withy 0.15 µM phalloidin (Thermofisher, Cat. No. A-31573, dissolved in 1x PBS pH 7.4) and incubated for 30 minutes. The wells were rinsed with 1x PBS (pH 7.4) and stored with 5 mM sodium azide before being visualized with the confocal imaging (Stellaris 5 Confocal LSM Leica). The obtained pictures were processed with FIJI.

Results

Electroporation optimization

To visualize RAW 264.7 cells expressing proteins of interest by microscopy in this project, the electroporation started with conditions in light of existing literatures (Stacey et al., 1993; Thompson et al., 1999), and where optimized by varying voltages and plasmid concentrations.

To assess the effect of voltage on cells viability, a mock experiment was designed. RAW264.7 cells showed minimal decrease in cell viability (75% to 80%) compared to the control group (0V, 89%) *Figure 1*), indicating that varying voltages had a minimal impact on cell viability.

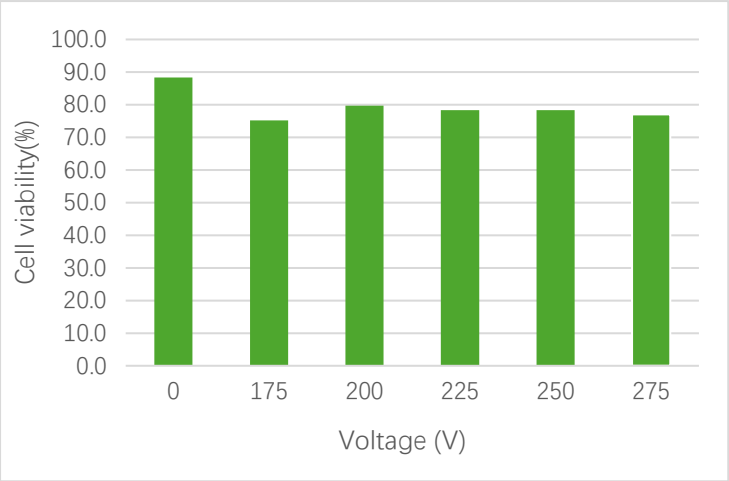

Figure 1. Cell viability 48 h after electroporation at various voltages. Cell viabilities were determined by the proportion of living cells within the total population.

To evaluate how varying plasmid quantities under 200 V and 275 V electrical conditions impacted cell viability, we used 3 µg, 10 µg, 20 µg eGFP plasmid per cuvette and a control group (no plasmid, subjected to 200 V). The 275 V / 10 µg plasmid condition yielded the highest eGFP expression (5%), outperforming all 200 V groups, which ranged from 1.4% to 1.8%. (*Figure 2*) (gating strategy: *Figure A2*).

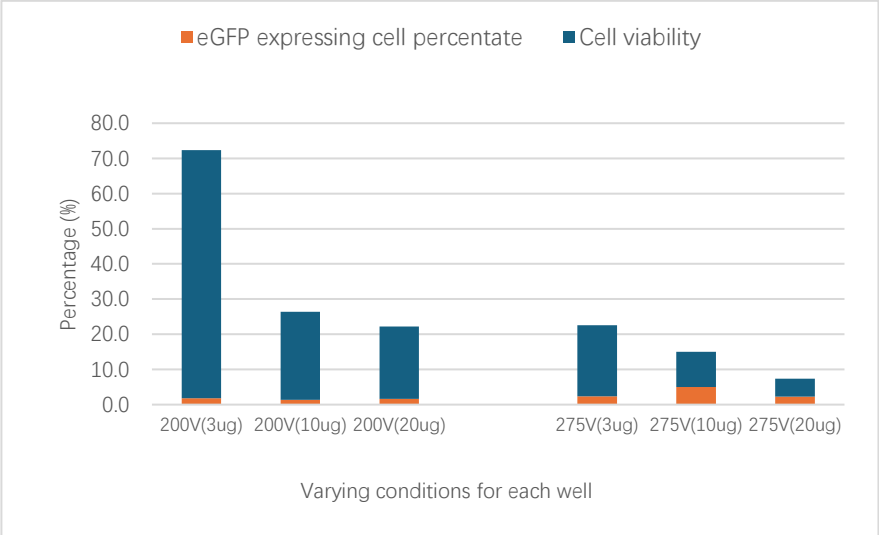

Figure 2. eGFP expressing cell percentage and cell viability at 200 V or 275 V with varying plasmid quantities. Cell viability and eGFP expression percentages calculated relative to the number of living cells in the control group.

To maximize eGFP expression, subsequent experiments used 10 µg plasmid per cuvette, and where subjected to either 250 V or 275 V electric shock. The percentages of cells expressing eGFP (from eGFP and eGFP-PLEKHO2 plasmids) were calculated as the ratio of eGFP-positive cells to total cells. The eGFP-PLEKHO2 plasmid groups showed higher expression levels compared to the eGFP plasmid groups under the same conditions (*Figure 3*). However, the highest expression ratio (7.5%) was

observed in the 250 V* (eGFP) group, which lacked a comparable eGFP-PLEKHO2 group. Ultimately, the conditions were set as 10 µg plasmid per cuvette with 5,000,000 cells/ml, subjected to a 250 V shock prior to cell straining (post-**electroporation**)

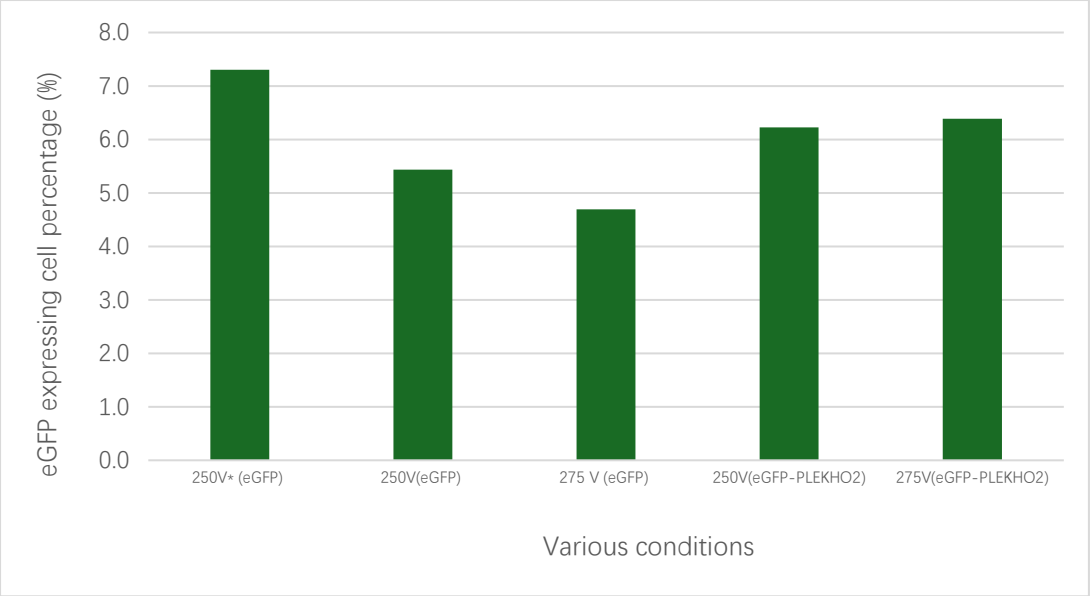

Figure 3. The percentage of eGFP(-PLEKHO2)-expressing cells treated with 10 µg plasmid per well and subjected to 250 V or 275 V electric shocks. The 250 V (eGFP) group underwent electroporation at 5,000,000 cells/ml in the cuvette (10,000,000 used in other groups).* Although the parameters could be further optimized, the efficiency was adequate for investigating protein localization for microscopy purposes. As a result, the established methodology was used throughout the remainder of this thesis.

PLEKHO2 was recruited to membrane and colocalize with accumulated F-actin in cups during phagocytosis

Following the protocol established in the first step, eGFP-PLEKHO2 plasmid was introduced into RAW 264.7 cells to track PLEKHO2 during phagocytosis. Using confocal microscope, localization of PLEKHO2 and F-actin in RAW cells were captured and visualized during phagocytosis.

We captured 17 eGFP-PLEKHO2-expressing RAW cells interacting with beads. 15 cells formed multiple phagocytic cups while engaging various beads except 2 RAW cells had completely internalized beads only. To separate stages of phagocytic cups, phagocytosis was categorized into early and late stages, with 50% bead internalization as the threshold (excluding complete internalization). The analysis comprised 14 early-stage and 6 late-stage phagocytic cups, with 6 RAW cells chosen to visually represent various-stage cups (*Figure 4*). In general, eGFP-PLEKHO2 and F-actin both concentrated in phagocytic cups, exhibiting subtle differences in their distribution patterns. During very early stage (*Figure 4*, 10% engulfment), PLEKHO2 exhibited a broader band of enrichment compared to the more focused F-actin localization upon initiation of phagocytosis. In a later stage (*Figure 4*, 50% engulfment),

PLEKHO2 positioned itself ahead of F-actin at the leading edge of the phagocytic cup, while co-localizing with F-actin in the remaining cup. Moreover, at advanced stages of engulfment (*Figure 4*, 80% engulfment), both F-actin and PLEKHO2 exhibited intensified concentration at the junction between two beads relative to other areas of the phagocytic cup. In fully formed phagosomes (*Figure 4*, 100% engulfment), F-actin and PLEKHO2 exhibited a similar distribution pattern: remaining assembled around one internalized bead while disassembling around the other. Among the 27 fully internalized beads analyzed, 21 exhibited complete disassembly of F-actin at the surrounding areas, except for one bead that retained F-actin accumulation along the cell membrane in contact with the bead. The remaining 6 beads showed F-actin and PLEKHO2 colocalization around beads. Besides, PLEKHO2 intensity decreased at sites where F-actin began to disassemble (*Figure 4*, 100% engulfment, the left bead), suggesting a functional dependency between their dissociation processes.

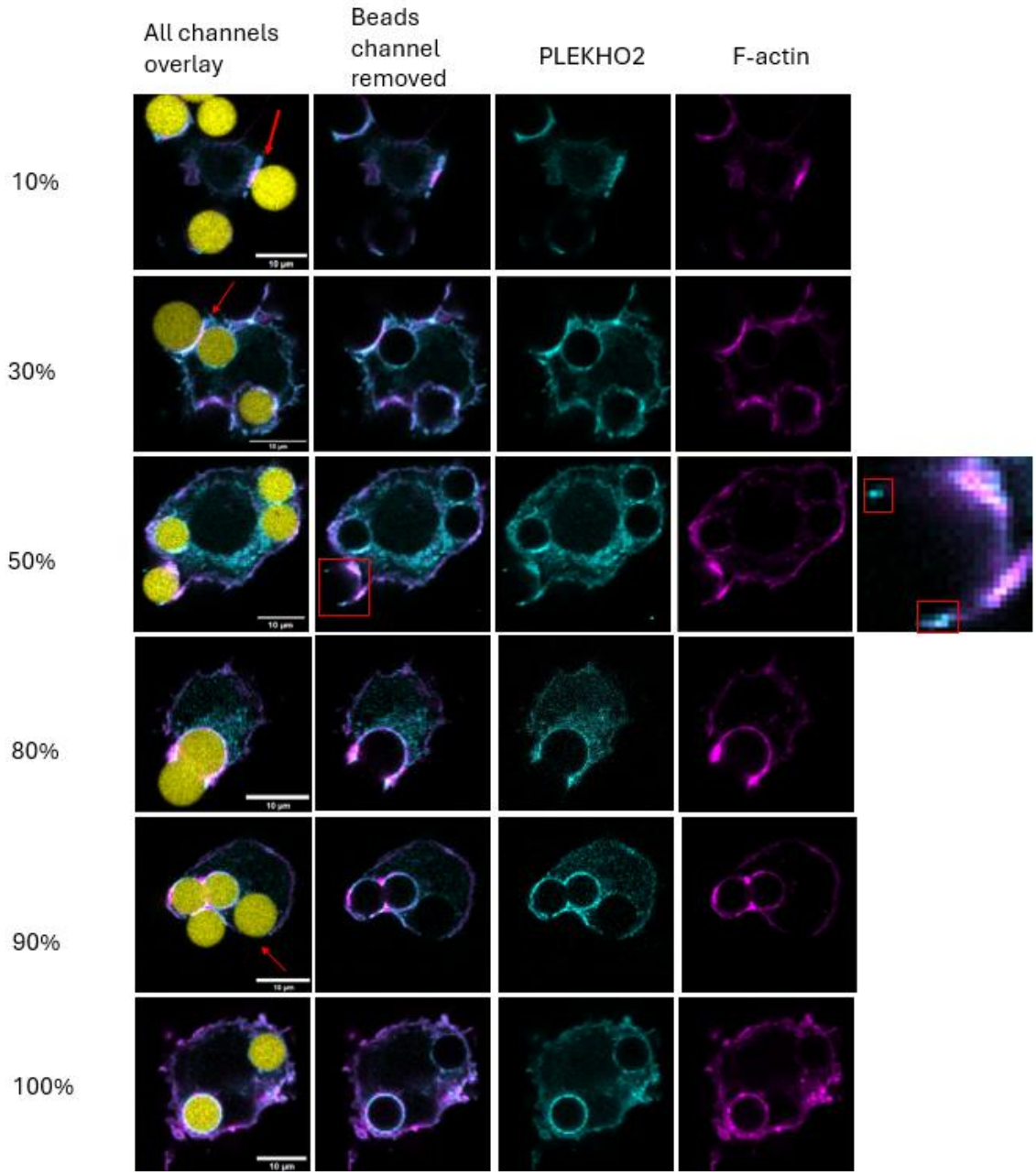

Figure 4. eGFP-PLEKHO2 (cyan)-transfected RAW 264.7 cells engulfing IgG functionalized DAAM-particles (yellow) and stained F-actin with alexafluor-647 phalloidin (magenta) for F-actin visualization. The percentages represented approximate engulfment extent. The red arrows indicate the focused cup in each image. The single image on the right column showed a magnified view of the phagocytic cup containing a 50% engulfed bead, highlighted by a red square.

To assess the colocalization between PLEKHO2 and F-actin, we employed a customized image processing method (*Figure 5*) prior to generating intensity profiles and computing the Pearson correlation coefficient (*Figure 6*). Fluorescence intensity profiles were smoothed using a 5-point moving average to reduce the noise.

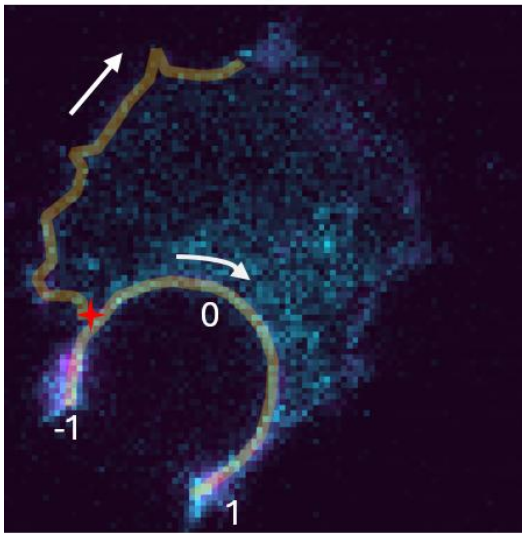

Figure 5. Indication example of protein intensity quantification in cell membrane and intensity normalization. To establish a baseline for fluorescence intensity measurements, a 15-micron segmented line was drawn from the cup base along the membrane, avoiding uneven areas (starting from the red star icon here). The "Plot Profile" function in FIJI was used to generate pixel intensity values along this line, with the average intensity serving as the baseline. Next, a segmented line was drawn along the cup from the left protrusion tip to the right, scaled from -1 to 1, with 0 marking the midpoint of the cup's length. The intensity values along the cup were obtained and then normalized using the corresponding baseline values. One channel each time. (Fully engulfed beads were excluded due to protrusions fusing)

Normalized intensity profiles quantified PLEKHO2 and F-actin colocalization in phagocytic cups at various stages (*Figure 6*), with Pearson correlation coefficients further validated their associations (*Table 1, Table A1*). The average coefficients between PLEKHO2 and F-actin at early and late stages indicated a consistent close association within phagocytic cups (*Table 1*).

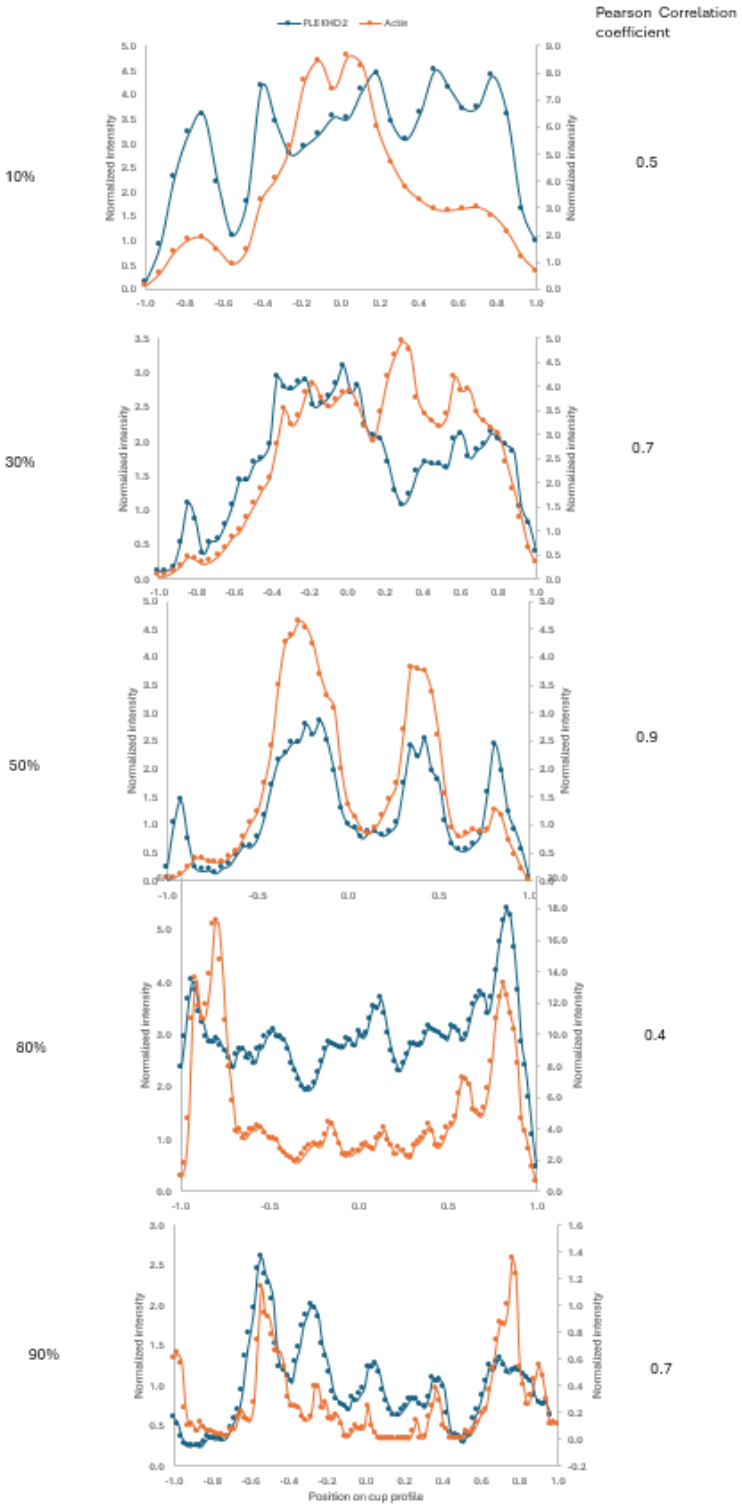

Figure 6. Normalized intensity profiles of F-actin (orange) and eGFP-PLEKHO2 (dark blue) along phagocytic cups, corresponding to cups in Figure 5. The x-axis represented the relative position along the cup (-1 to 1), and the y-axes (left one for PLEKHO2, right one for F-actin) shows normalized fluorescence intensity. The right column: Pearson correlation coefficients of each cup.

Table 1. Pearson correlation coefficient between F-actin and protein of interest, with n representing the

sample size.

cc	PLEKHO2	CAPZA	PIP2
Early stage	0.7(n=14)	0.8(n=7)	0.7(n=8)
Late stage	0.6 (n=6)	0.8(n=5)	0.5(n=4)
Average	0.7(n=20)	0.8(n=12)	0.6(n=12)

In conclusion, PLEKHO2 was recruited to macrophage membrane during phagocytosis observed in various stages, coinciding with F-actin accumulation in phagocytic cups.

CAPZA showed similar localization as PLEKHO2 in phagocytic cups, while PIP2 accumulated transiently during early stages.

To infer whether PLEKHO2 colocalized with CAPZA/PIP2 during phagocytosis, CAPZA was tracked directly in cells following the same protocol established, while PIP2 was tracked by a reporter protein with binding-affinity to PIP2.

12 CAPZA cells were imaged, from which 12 phagocytic cups were selected for analysis. CAPZA showed similar intensity in the cell membrane and cytoplasm, except in phagocytic cups. It accumulated in cups at various discrete stages observed, from initiation to complete engulfment (*Figures 7, 8*), indicating a strong link to the phagocytic process. Unlike the partial colocalization of PLEKHO2 and F-actin observed in two RAW cells, CAPZA and F-actin demonstrated complete overlap in all 12 phagocytic cups analyzed through microscopy, including the area surrounding the fully internalized bead (*Figure.7*, 100% engulfment). Combining with correlation coefficients of CAPZA and F-actin (*Table. 1*), also the intensity profiles (*Figure. 8*), a close association during phagocytosis was identified.

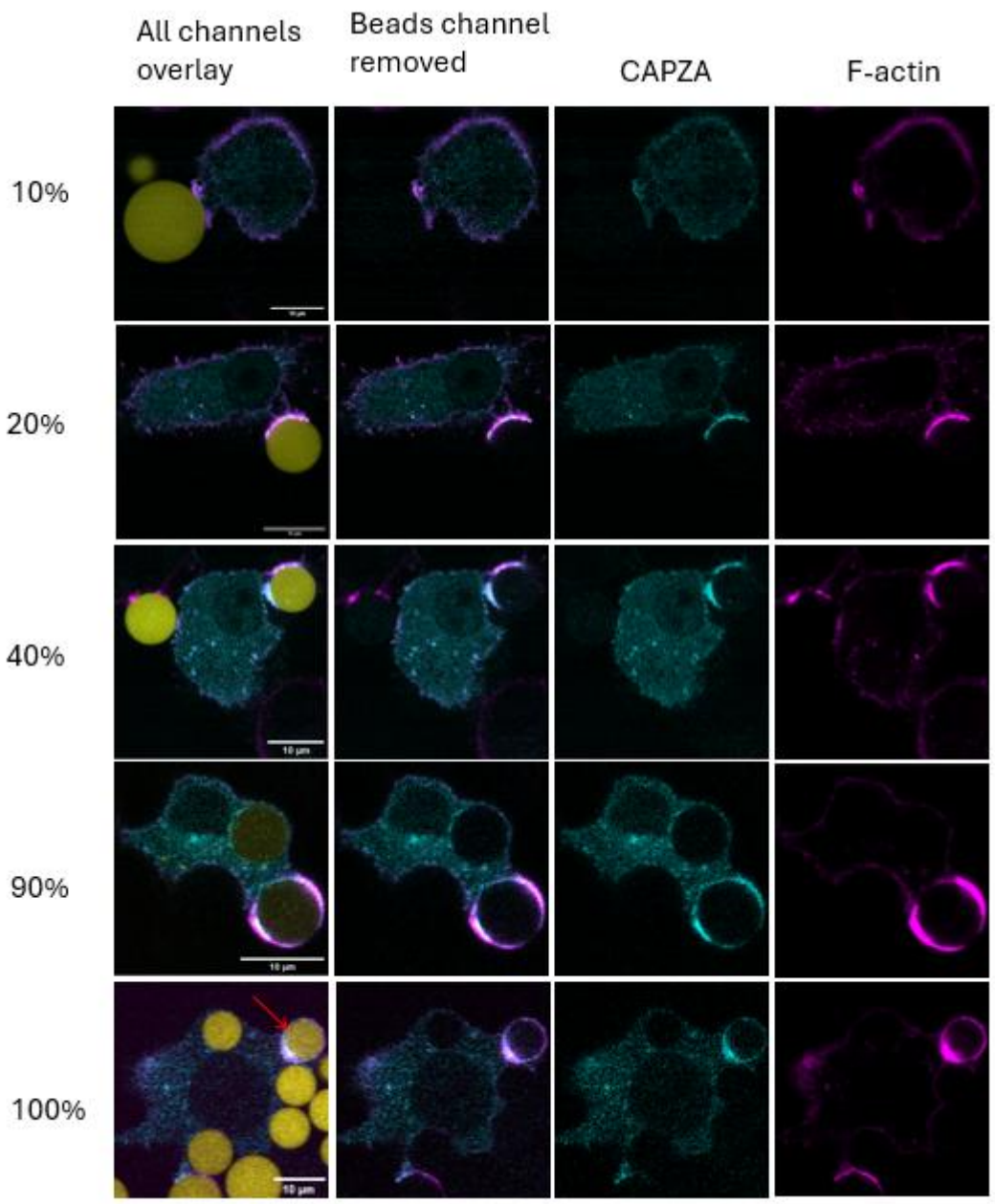

Figure 7. YFP-CAPZA (cyan)-transfected RAW 264.7 cells engulfing IgG functionalized DAAM-particles (yellow) and stained with alexafluor-647 phalloidin (magenta) for F-actin visualization.

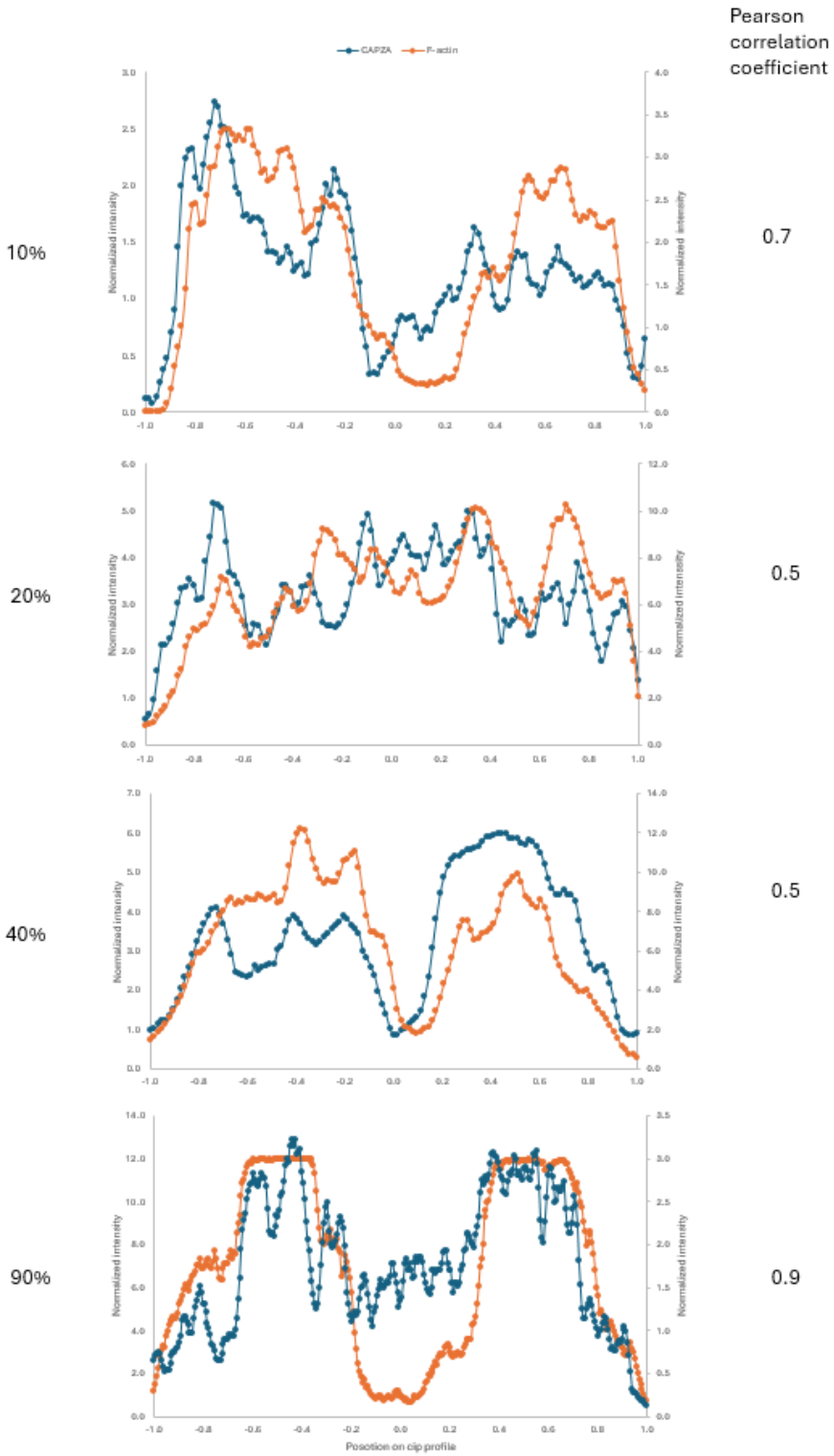

Figure 8. Normalized intensity profiles of F-actin (orange) and CAPZA (dark blue) along phagocytic cups, corresponding to cups in Figure. 7.

PIP2 exhibited higher concentration in the cell membrane relative to its cytoplasmic distribution (*Figure 9*). This membrane enrichment was also noticeable in early-stage phagocytic cups, as observed in cups with 20% and 40% engulfment (*Figure. 9*), confirmed by the normalized intensity profiles (*Figure. 10*).

At late-stage phagocytosis (*Figure. 9,* 80% engulfment), PIP2 enrichment in the front protrusion area was less pronounced than F-actin. Intensity profiles revealed a slight PIP2 accumulation in this area (maximum normalized intensity: 1.3), exhibiting a more stable trend compared to the F-actin profile (*Figure 10*), which showed two distinct spikes with maximum 9.5 normalized intensity (the baseline y=1, representing average membrane intensity). PIP2 and F-actin colocalization, initially high in early-stage phagocytic cups (coefficient = 0.7; *Table 1, Figure 10*), decreased in late-stage cups (coefficient = 0.5) as PIP2 levels diminished despite persistent F-actin, thus indicating PIP2's transient accumulation during early-stage phagocytosis. Notably, PIP2 accumulation was evident in intensity profiles, but in general to a lesser extent than PLEKHO2 and CAPZA. Its levels were only slightly above the baseline (y<2).

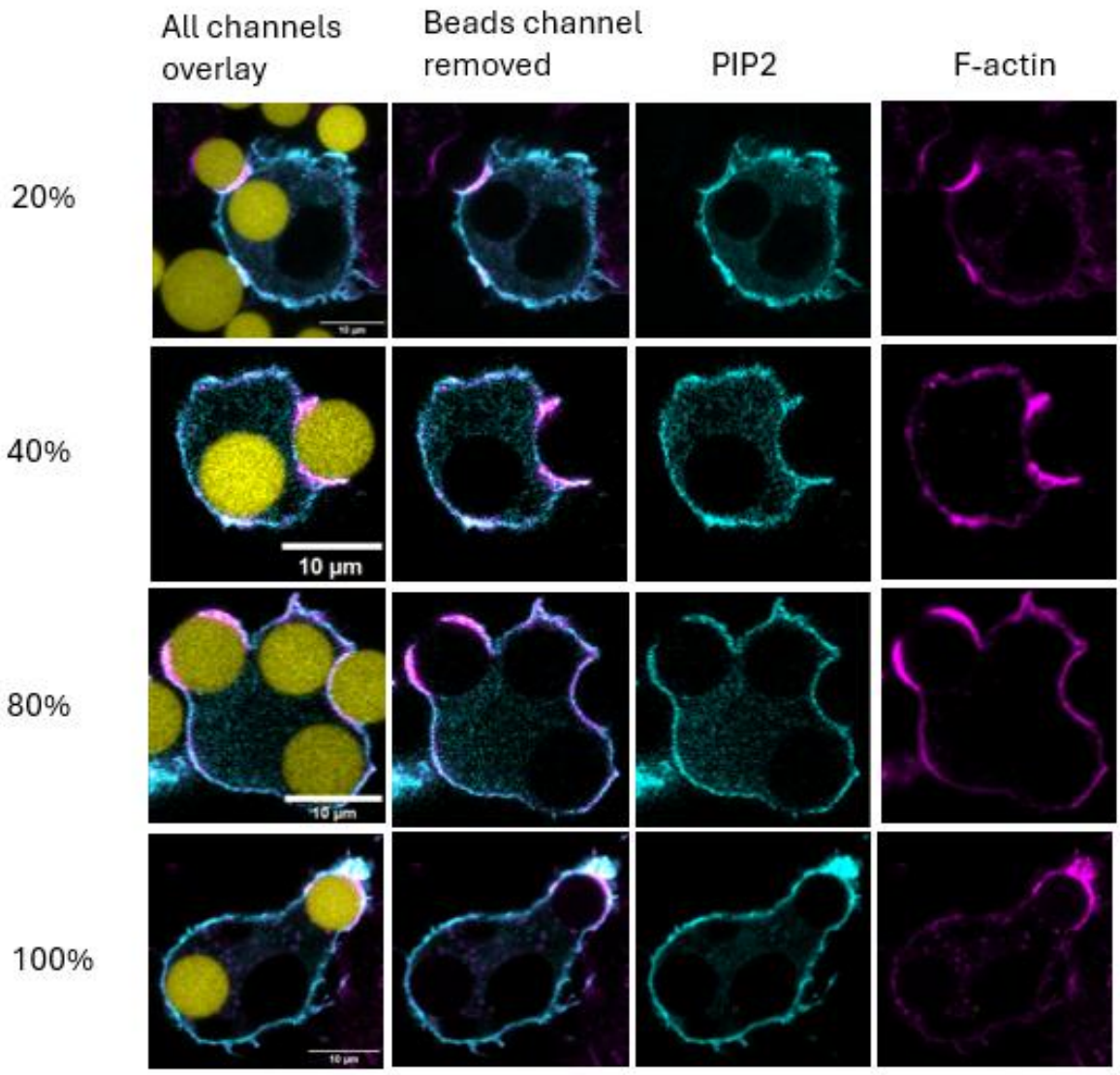

Figure 9. eGFP-PLCδ-PH (cyan)-transfected RAW 264.7 cells engulfing IgG functionalized DAAM-particles (yellow) and stained with alexafluor-647 phalloidin (magenta) for F-actin visualization.

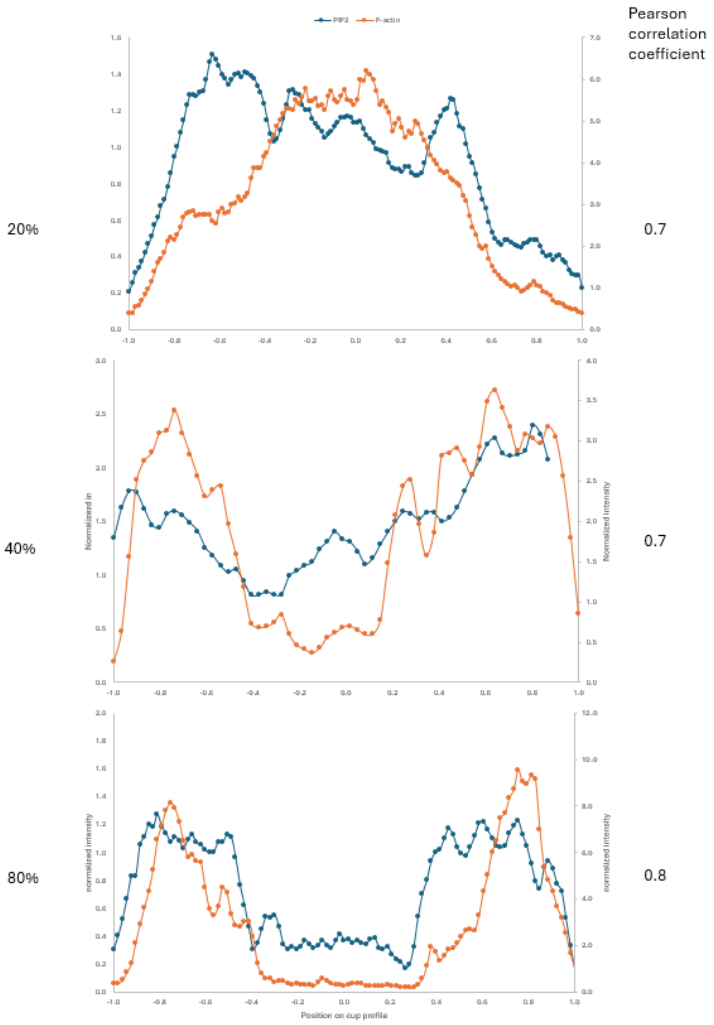

Figure 10. Spatial distribution and correlation of F-actin and PIP2 in phagocytic cups. Normalized intensity profiles of F-actin (orange) and PIP2 (dark blue) along phagocytic cups, corresponding to cups in Figure X.

In conclusion, CAPZA was observed to accumulate in cups alongside F-actin intensification in various phagocytic stages by microscopy and supported by Pearson correlation coefficients. Its distribution pattern with F-actin paralleled the pattern of PLEKHO2 with F-actin. Furthermore, both microscopy images and Pearson correlation coefficients suggested that PIP2 showed enhanced distribution and colocalization with F-actin in early-stage phagocytic cups, but dissociated from F-actin in late-stage cups.

Discussion

Phosphoinositide-binding Pleckstrin homology domains were recognized for their crucial role in a variety of cellular processes. This study established a methodology to investigate individual protein localization in macrophages during phagocytosis using electroporation and fluorescence visualization, focusing on PLEKHO2 and CAPZA. Additionally, using the PIP2 reporter (PLCδ-PH), we examined

whether PLEKHO2 and CAPZA colocalized with the phagocytosis-associated phosphoinositol lipid PIP2. PLEKHO2 and CAPZA colocalized with F-actin in phagocytic cups at various stages of engulfment, suggesting their involvement throughout phagocytosis. Raw cells expressing the PIP2 reporter exhibited a transient accumulation of PIP2 during the early stages of phagocytosis, where it colocalized with F-actin in the phagocytic cups. However, during the later stages, PIP2 detached from the phagocytic cups and showed reduced colocalization with F-actin.

Existing research demonstrated the important role of PLEKHO2 in cell survival regulation with the molecular pathway remaining elusive (Zhang et al., 2017; Zhou et al., 2021). Our study revealed PLEKHO2's role in phagocytosis by demonstrating its co-localization with F-actin at various stages of phagocytic cup formation. A possible explanation for PLEKHO2 positioning ahead of F-actin at the protrusion tip was its recruitment to the membrane where phagocytosis initiates. This localization was likely facilitated by the PH domain of PLEKHO2, which can target specific membrane regions by interacting with phosphoinositides (Lemmon, 2007; Lemmon et al., 2002; Powis et al., 2023). Membrane advancing protrusions, driven by F-actin-based force, ruffled the membrane (accumulated PLEKHO2 embedded) while leaving F-actin branches slightly spatially behind the tips leading to a "sandwich" structure (PLEKHO2-F-actin-PLEKHO2) on the surface of beads. This phenomenon was not visualized in all the images captured, it could be due to angles of protrusion or object magnification limitations. For RAW cells with fully internalized beads, F-actin was observed to be recruited around the beads in the captured moment. This observation aligns with F-actin flashes, which are known to be transient recruitment of F-actin on phagosomes occurring shortly after internalization. However, as this was not a real-time observation, it likely captured one instance of these dynamic F-actin accumulations (Poirier et al., 2020). Notably, the accumulation of PLEKHO2 showed a spatial correlation with F-actin recruitment around the internalized beads (*Figure 4*). Potentially, PLEKHO2 was "stuck" between beads and F-actin layer, referring to the "sandwich" structure, which might be caused by the effect of electroporation or PLEKHO2 overexpression (compared to endogenous level) by introducing plasmid.

We observed complete overlaps of CAPZA and F-actin distributions at various stages of cup formation (*Figure 7, 8*), suggesting a close relationship between those proteins during phagocytosis. We originally hypothesized CAPZA localization slightly behind protrusion tips during phagocytosis, given its role in capping the fast-growing ends of F-actin branches (Cooper & Sept, 2008; Jaumouille & Waterman, 2020; Mylvaganam et al., 2021). However, the subtle localization differences may be beyond confocal microscopy resolution. Briefly, our study supported the previously predicted interaction between PLEKHO2 and CAPZA by demonstrating similar distribution patterns of both proteins with F-actin. (Cho et al., 2022)

PIP2 enriches in the inner leaflet of the plasma membrane, playing crucial roles in various cellular processes (Rajala & Anderson, 2010), including phagocytosis (Scott et al., 2005; Tuosto et al., 2015). Indeed, PIP2 showed intensified localization in cell membrane (*Figure 9, 10)* compared to cytoplasmic distribution. PIP2 was reported to undergo focal accumulation in the inner leaflet of the phagosomal

cup at the onset of phagocytosis (Tuosto et al., 2015), serving as a scaffold for proteins like profilin, cofilin, talin, vinculin, WASP, and ERM family proteins (ezrin/moesin/radixin), which drive F-actin filament assembly and membrane protrusion (Johnson & Rodgers, 2008; Tuosto et al., 2015). PIP2 rapidly disappears from the base of cups before sealing which closely paralleled the spatial and temporal pattern of F-actin disassembly during phagocytosis (Scott et al., 2005). During late stage, hydrolysis of PIP2 by PLCγ reduces PIP2 levels, releasing cofilin from PIP2-mediated inhibition. Activated cofilin then severs F-actin, enabling cytoskeletal disassembly and phagosome scission (Golebiewska et al., 2011; Rotshenker, 2022; van Rheenen & Jalink, 2002). In this study, the correlation coefficient and microscopy results of PIP2 and F-actin presented the same trend during phagocytosis, as mentioned above.

Based on the findings of this study, several potential improvements to the methodology have been identified for future research: the ratio of cells and beads for microscopy imaging was originally aimed at "one bead per cell" to allow accurate analysis (Cannon & Swanson, 1992), and yet the optimization was not realized due to time limitations. To accurately assess colocalization, both proteins should be simultaneously visualized within the same cell. However, the chance of visualizing a cell expressing two introduced plasmids is very low due to factors such as low co-transformation efficiency (Tomoiaga et al., 2022), and potential plasmid incompatibility (Lee & Ko, 2021). Methods could be developed such as using fluorescent antibody to specifically bind CAPZA in PLEKHO2 plasmid-introduced cells (Sosnik et al., 2010). Additionally, RAW cells often clump following electroporation, making it crucial to de-clump them before seeding for microscopy to ensure proper cell density. To further substantiate the hypothesized high binding affinity between PLEKHO2 and phosphatidylinositol, future studies should consider the dynamics of both PIP2 and its derivative, phosphatidylinositol 3,4,5-trisphosphate (PIP3). PIP3 is generated from PIP2 through hydrolysis by PLCγ and subsequent phosphorylation by PI3K (Tariq & Luikart, 2021). Examining the concurrent changes in both lipids during phagocytosis may provide a more comprehensive understanding of PLEKHO2's interactions with phosphatidylinositols.

In a wider scope, further follow-up investigation on the underlying mechanisms of its function could be conducted, as the participance of PLEKHO2 in phagocytosis was validated in this study. The structure of PLEKHO2 might be worth defining first as structure of protein is essential for function prediction. Next, PLEKHO2 has been demonstrated to be critical for macrophage survival, particularly in response to M-CSF signaling (Zhang et al., 2017). Further studies could explore how PLEKHO2's impact on macrophage survival affects phagocytosis. Research might investigate whether PLEKHO2-deficient macrophages, due to compromised viability, show reduced ability to engulf and process pathogens or apoptotic cells. A potential experimental approach would involve using PLEKHO2-knockout macrophages to quantify the uptake and digestion of opsonized particles or apoptotic cells, comparing their performance to wild-type controls. Additionally, PLEKHO2 expression was reported to increase during macrophage differentiation and maturation though the underlying pathway remains unclear

(Zhang et al., 2017), presenting an opportunity for further exploration. Regarding implications for disease aspect, since downregulation of PLEKHO2 correlates with impaired macrophage function in sepsis-induced ARDS (Zhang et al., 2017), future research could evaluate whether restoring PLEKHO2 expression can rescue defective phagocytosis in these conditions by gene therapy approaches.

In conclusion, in this thesis a protocol for electroporating RAW 264.7 cell-line to localize proteins in phagocytes during phagocytosis was optimized. The findings revealed that PLEKHO2 plays a role in the phagocytosis process, aligning with the accumulation of F-actin observed at different phases of phagocytic cup formation. Additionally, the results suggest a possible close association between PLEKHO2 and CAPZA. In general, this research laid a foundation for further studies into PLEKHO2. Ultimately, unraveling PLEKHO2's role in phagocytosis seeks to offer a clearer understanding of this protein's function, potentially revealing its specific molecular pathways. This knowledge could lead to the identification of new therapeutic targets for conditions marked by defective phagocytosis, including sepsis and neurodegenerative diseases.

References

Aderem, A., & Underhill, D. M. (1999). Mechanisms of phagocytosis in macrophages. *Annu Rev Immunol*, *17*, 593-623. https://doi.org/10.1146/annurev.immunol.17.1.593

Boada-Romero, E., Martinez, J., Heckmann, B. L., & Green, D. R. (2020). The clearance of dead cells by efferocytosis. *Nat Rev Mol Cell Biol*, *21*(7), 398-414. https://doi.org/10.1038/s41580-020-0232-1

C. Han, E., Huang, Y.-C., Lin, J.-M., Lin, H.-J., Wu, J.-Y., Lee, C.-C., & Tsai, F.-J. (2012). Association of the PLEKHO2 and PLEKHH1 gene polymorphisms with type 2 diabetic retinopathy in a Taiwanese population. *ScienceAsia*, *38*(4), 340. https://doi.org/10.2306/scienceasia1513-1874.2012.38.340

Cannon, G. J., & Swanson, J. A. (1992). The macrophage capacity for phagocytosis. *J Cell Sci*, *101 (Pt 4)*, 907-913. https://doi.org/10.1242/jcs.101.4.907

Cho, N. H., Cheveralls, K. C., Brunner, A. D., Kim, K., Michaelis, A. C., Raghavan, P., Kobayashi, H., Savy, L., Li, J. Y., Canaj, H., Kim, J. Y. S., Stewart, E. M., Gnann, C., McCarthy, F., Cabrera, J. P., Brunetti, R. M., Chhun, B. B., Dingle, G., Hein, M. Y.,…Leonetti, M. D. (2022). OpenCell: Endogenous tagging for the cartography of human cellular organization. *Science*, *375*(6585), eabi6983. https://doi.org/10.1126/science.abi6983

Cooper, J. A., & Sept, D. (2008). New insights into mechanism and regulation of actin capping protein. *Int Rev Cell Mol Biol*, *267*, 183-206. https://doi.org/10.1016/S1937-6448(08)00604-7

Donnelly, L. E., & Barnes, P. J. (2012). Defective phagocytosis in airways disease. *Chest*, *141*(4), 1055-1062. https://doi.org/10.1378/chest.11-2348

Edwards, M. (2014). Capping Protein Regulators Fine-Tune Actin Assembly Dynamics. *29*.

Galloway, D. A., Phillips, A. E. M., Owen, D. R. J., & Moore, C. S. (2019). Phagocytosis in the Brain: Homeostasis and Disease. *Frontiers in Immunology*, *10*. https://doi.org/10.3389/fimmu.2019.00790

Gillooly, D. J., Simonsen, A., & Stenmark, H. (2001). Phosphoinositides and phagocytosis. *J Cell Biol*, *155*(1), 15-17. https://doi.org/10.1083/jcb.200109001

Golebiewska, U., Kay, J. G., Masters, T., Grinstein, S., Im, W., Pastor, R. W., Scarlata, S., & McLaughlin, S. (2011). Evidence for a fence that impedes the diffusion of phosphatidylinositol 4,5-bisphosphate out of the forming phagosomes of macrophages. *Mol Biol Cell*, *22*(18), 3498-3507. https://doi.org/10.1091/mbc.E11-02-0114

Hirayama, D., Iida, T., & Nakase, H. (2017). The Phagocytic Function of Macrophage-Enforcing Innate Immunity and Tissue Homeostasis. *International Journal of Molecular Sciences*, *19*(1), 92. https://doi.org/10.3390/ijms19010092

Jaumouille, V., & Waterman, C. M. (2020). Physical Constraints and Forces Involved in Phagocytosis. *Front Immunol*, *11*, 1097. https://doi.org/10.3389/fimmu.2020.01097

Johnson, C. M., & Rodgers, W. (2008). Spatial Segregation of Phosphatidylinositol 4,5-Bisphosphate (PIP(2)) Signaling in Immune Cell Functions. *Immunol Endocr Metab Agents Med Chem*, *8*(4), 349-357. https://doi.org/10.2174/187152208787169233

Lee, H., & Ko, K. S. (2021). Effect of multiple, compatible plasmids on the fitness of the bacterial host by inducing transcriptional changes. *J Antimicrob Chemother*, *76*(10), 2528-2537. https://doi.org/10.1093/jac/dkab240

Lemmon, M. A. (2007). Pleckstrin homology (PH) domains and phosphoinositides. *Biochem Soc Symp*(74), 81-93. https://doi.org/10.1042/BSS0740081

Lemmon, M. A., Ferguson, K. M., & Abrams, C. S. (2002). Pleckstrin homology domains and the cytoskeleton. *FEBS Letters*, *513*(1), 71-76. https://doi.org/10.1016/s0014-5793(01)03243-4

Lemmon, M. A., Ferguson, K. M., & Schlessinger, J. (1996). PH domains: diverse sequences with a common fold recruit signaling molecules to the cell surface. *Cell*, *85*(5), 621-624. https://doi.org/10.1016/s0092-8674(00)81022-3

Levin, R., Grinstein, S., & Schlam, D. (2015). Phosphoinositides in phagocytosis and macropinocytosis. *Biochim Biophys Acta*, *1851*(6), 805-823. https://doi.org/10.1016/j.bbalip.2014.09.005

Mylvaganam, S., Freeman, S. A., & Grinstein, S. (2021). The cytoskeleton in phagocytosis and macropinocytosis. *Curr Biol*, *31*(10), R619-R632. https://doi.org/10.1016/j.cub.2021.01.036

Poirier, M. B., Fiorino, C., Rajasekar, T. K., & Harrison, R. E. (2020). F-actin flashes on phagosomes mechanically deform contents for efficient digestion in macrophages. *J Cell Sci*, *133*(12). https://doi.org/10.1242/jcs.239384

Powis, G., Meuillet, E. J., Indarte, M., Booher, G., & Kirkpatrick, L. (2023). Pleckstrin Homology [PH] domain, structure, mechanism, and contribution to human disease. *Biomed Pharmacother*, *165*, 115024. https://doi.org/10.1016/j.biopha.2023.115024

Rotshenker, S. (2022). Galectin-3 (MAC-2) controls phagocytosis and macropinocytosis through intracellular and extracellular mechanisms. *Front Cell Neurosci*, *16*, 949079. https://doi.org/10.3389/fncel.2022.949079

Scott, C. C., Dobson, W., Botelho, R. J., Coady-Osberg, N., Chavrier, P., Knecht, D. A., Heath, C., Stahl, P., & Grinstein, S. (2005). Phosphatidylinositol-4,5-bisphosphate hydrolysis directs actin remodeling during phagocytosis. *J Cell Biol*, *169*(1), 139-149. https://doi.org/10.1083/jcb.200412162

Sosnik, J., Buffone, M. G., & Visconti, P. E. (2010). Analysis of CAPZA3 localization reveals temporally discrete events during the acrosome reaction. *J Cell Physiol*, *224*(3), 575-580. https://doi.org/10.1002/jcp.22211

Stacey, K. J., Ross, I. L., & Hume, D. A. (1993). Electroporation and DNA-dependent cell death in murine macrophages. *Immunol Cell Biol*, *71 (Pt 2)*, 75-85. https://doi.org/10.1038/icb.1993.8

Tariq, K., & Luikart, B. W. (2021). Striking a balance: PIP(2) and PIP(3) signaling in neuronal health and disease. *Explor Neuroprotective Ther*, *1*, 86-100. https://doi.org/10.37349/ent.2021.00008

Thompson, C. D., Frazier-Jessen, M. R., Rawat, R., Nordan, R. P., & Brown, R. T. (1999). Evaluation of Methods for Transient Transfection of a Murine Macrophage Cell Line, RAW 264.7. *BioTechniques*, *27*(4), 824-832. https://doi.org/10.2144/99274rr05

Tomoiaga, D., Bubnell, J., Herndon, L., & Feinstein, P. (2022). High rates of plasmid cotransformation in E. coli overturn the clonality myth and reveal colony development. *Sci Rep*, *12*(1), 11515. https://doi.org/10.1038/s41598-022-14598-9

Tuosto, L., Capuano, C., Muscolini, M., Santoni, A., & Galandrini, R. (2015). The multifaceted role of PIP2 in leukocyte biology. *Cell Mol Life Sci*, *72*(23), 4461-4474. https://doi.org/10.1007/s00018-015-2013-0

Uribe-Querol, E., & Rosales, C. (2024). Phagocytosis. *Methods Mol Biol*, *2813*, 39-64. https://doi.org/10.1007/978-1-0716-3890-3_3

van Rheenen, J., & Jalink, K. (2002). Agonist-induced PIP(2) hydrolysis inhibits cortical actin dynamics: regulation at a global but not at a micrometer scale. *Mol Biol Cell*, *13*(9), 3257-3267. https://doi.org/10.1091/mbc.e02-04-0231

Vieira, O. V., Botelho, R. J., Rameh, L., Brachmann, S. M., Matsuo, T., Davidson, H. W., Schreiber, A., Backer, J. M., Cantley, L. C., & Grinstein, S. (2001). Distinct roles of class I and class III phosphatidylinositol 3-kinases in phagosome formation and maturation. *J Cell Biol*, *155*(1), 19-25. https://doi.org/10.1083/jcb.200107069

Vorselen, D., Kamber, R. A., Labitigan, R. L. D., Van Loon, A. P., Peterman, E., Delgado, M. K., Lin, S., Rasmussen, J. P., Bassik, M. C., & Theriot, J. A. (2022). *Cell surface receptors TREM2, CD14 and integrin α_Mβ₂drive sinking engulfment in phosphatidylserine-mediated phagocytosis*. Cold Spring Harbor Laboratory. https://dx.doi.org/10.1101/2022.07.30.502145

https://www.biorxiv.org/content/biorxiv/early/2022/07/31/2022.07.30.502145.full.pdf

Vorselen, D., Wang, Y., de Jesus, M. M., Shah, P. K., Footer, M. J., Huse, M., Cai, W., & Theriot, J. A. (2020). Microparticle traction force microscopy reveals subcellular force exertion patterns in immune cell-target interactions. *Nat Commun*, *11*(1), 20. https://doi.org/10.1038/s41467-019-13804-z

Wiggins, D. A., Maxwell, J. N., & Nelson, D. E. (2024). Exploring the role of CITED transcriptional regulators in the control of macrophage polarization. *Front Immunol*, *15*, 1365718. https://doi.org/10.3389/fimmu.2024.1365718

Yang, S., Du, P., Cui, H., Zheng, M., He, W., Gao, X., Hu, Z., Jia, S., Lu, Q., & Zhao, M. (2023). Regulatory factor X1 induces macrophage M1 polarization by promoting DNA demethylation in autoimmune inflammation. *JCI Insight*, *8*(20). https://doi.org/10.1172/jci.insight.165546

Zhang, P., Zhou, C., Lu, C., Li, W., Li, W., Jing, B., Chen, W., Zha, Y., Zhang, P., Bai, C., Liu, H., & Zhang, L. (2017). PLEKHO2 is essential for M-CSF-dependent macrophage survival. *Cell Signal*, *37*, 115-122. https://doi.org/10.1016/j.cellsig.2017.06.006

Zhou, C., Zhang, X., Yang, C., He, Y., & Zhang, L. (2021). PLEKHO2 inhibits TNFalpha-induced cell death by suppressing RIPK1 activation. *Cell Death Dis*, *12*(8), 714. https://doi.org/10.1038/s41419-021-04001-2

Appendix A

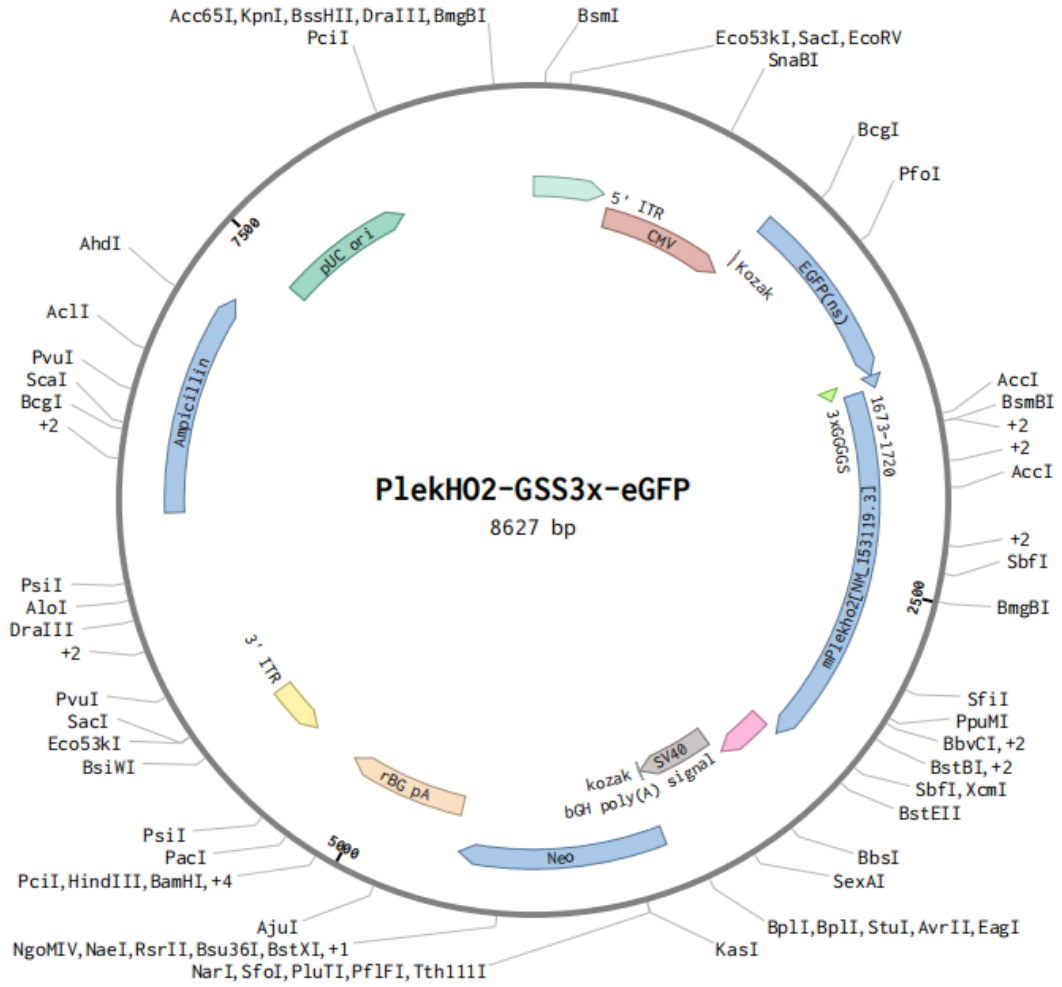

Figure A1. PlekHO2-GSS3x-eGFP (8627 bp) plasmid design. https://benchling.com/s/seq-plXTnkMK5CFLQI08Yt5Q/edit?m=slm-GDQ652EGzFeeb2f7vQr2

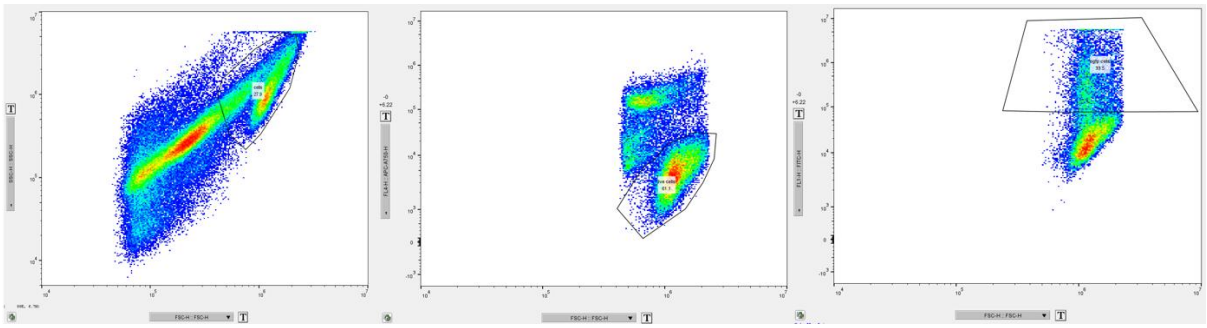

Figure A2. Gating strategy for flow cytometry analysis of eGFP/YFP cells of viable cells. Forward scatter (FSC) and side scatter (SSC) plots were employed to distinguish target cells from debris, followed by fluorescence-based gating to refine the selection of subpopulations for further analysis.

Table A1. Pearson correlation coefficient between F-actin and PLEKHO2/CAPZA/PIP2. The calculation was based on normalized intensity of F-actin and smoothed normalized intensity of the other protein in phagocytic cups.

	Approximate Engulment percentage(%)	Correlation efficient
PLEKHO2 cell	10	0.5
	25	0.7
	30	0.8
	33	0.7
	33	0.7
	34	0.8
	38	0.8
	40	0.7
	41	0.6
	42	0.9
	43	0.8
	45	0.7
	45	0.9
	47	0.8
	58	0.9
	60	0.6
	70	0.5
	70	0.9
	75	0.4
	80	0.5
CAPZA cell	15	0.7
	25	1.0
	34	0.5
	35	1.0
	40	0.8
	40	0.8
	50	0.6
	50	0.7
	60	0.7
	80	0.9
	81	0.9
	81	0.9
PIP2 reporter expressing cell	30	0.7
	30	0.6
	30	0.7
	40	0.6
	40	0.8
	42	0.6
	45	0.6
	50	0.7
	54	0.2
	60	0.7
	85	0.8
	85	0.4